Chemical Bonding in Actinyl (V/VI) Dipyriamethyrin Complexes for the Actinide Series from Americium to Californium: A Computational Investigation

Journal:	*Dalton Transactions*
Manuscript ID	DT-ART-04-2022-001142.R1
Article Type:	Paper
Date Submitted by the Author:	19-May-2022
Complete List of Authors:	Jennifer G, Abigail; SRM Institute of Science and Technology, Chemistry Gao, Yang; University Of Manitoba Department of Chemistry, Schreckenbach, Georg; University of Manitoba, Chemistry Varathan, E.; SRM Institute of Science and Technology, Department of Chemistry

Chemical Bonding in Actinyl (V/VI) Dipyriamethyrin Complexes for the Actinide Series from Americium to Californium: A Computational Investigation

Abigail Jennifer G.[1], Yang Gao[2,3,4], Georg Schreckenbach[2]* and Elumalai Varathan[1]*

[1]Department of Chemistry, SRM Institute of Science and Technology, Kattankulathur, Chennai 603203, Tamil Nadu, India.
[2]Department of Chemistry, University of Manitoba, Winnipeg, Manitoba, R3T 2N2, Canada.
[3]Institut National de La Recherche Scientifique (INRS)-Centre Énergie Matériaux Télécommunications, Varennes, QC, J3X 1P7, Canada.
[4]Institute of Fundamental and Frontier Sciences, University of Electronic Science and Technology of China, Chengdu, Sichuan 610054, China.
Email: schrecke@cc.umanitoba.ca
varathan.elumalai85@gmail.com, varathae@srmist.edu.in

ABSTRACT

The separation of minor actinides in their dioxocation (i.e., actinyl) form in high-valent oxidation states requires efficient ligands for their complexation. In this work, we evaluate the complexation properties of actinyls including americyl, curyl, berkelyl, and californyl in their pentavalent and hexavalent oxidation states with the dipyriamethyrin ligand (L) using density functional theory calculations. The calculated bond parameters show shorter An=O_{yl} bonds with covalent character and longer An-N bonds with ionic character. The bonding between actinyl cation and ligand anion shows a flow of charges from the ligand to actinyl in all $[An^{V/VI}O_2\text{-}L]^{1-/0}$ complexes. However, across the series backdonation of charges from metal to ligand becomes prominent and stabilizes the complexes. The thermodynamic parameters in the gas phase and solution suggest that the complex formation reaction is spontaneous for $[Cf^{V/VI}O_2\text{-}L]^{1-/0}$ complexes and spontaneous at elevated temperatures (>298.15K) for all other complexes. Spin-orbit corrections have a quantitative impact while the overall trend remains the same. The energy decomposition analysis (EDA) reveals that the interaction between actinyl and the ligand is mainly due to electrostatic contributions that decrease from Am to Cf along with an increase in orbital contributions due to the backdonation of charges from the actinyl metal center to the ligand that greatly stabilizes the Cf complex. The repulsive

Pauli energy contribution is observed to increase in the case of $[An^{V}O_2\text{-}L]^{1-}$ complexes from Am to Cf while a decrease is observed among $[An^{VI}O_2\text{-}L]^{0}$ complexes, showing minimum repulsion in the $[Cf^{VI}O_2\text{-}L]^{0}$ complex formation. Overall, the hexavalent actinyl complexes show greater stability (increasing from Am to Cf) than their pentavalent counterparts.

KEYWORDS: High Valent Actinyl, Actinyl Complexes, Energy Decomposition Analysis, ETS-NOCV, QTAIM.

GRAPHICAL ABSTRACT:

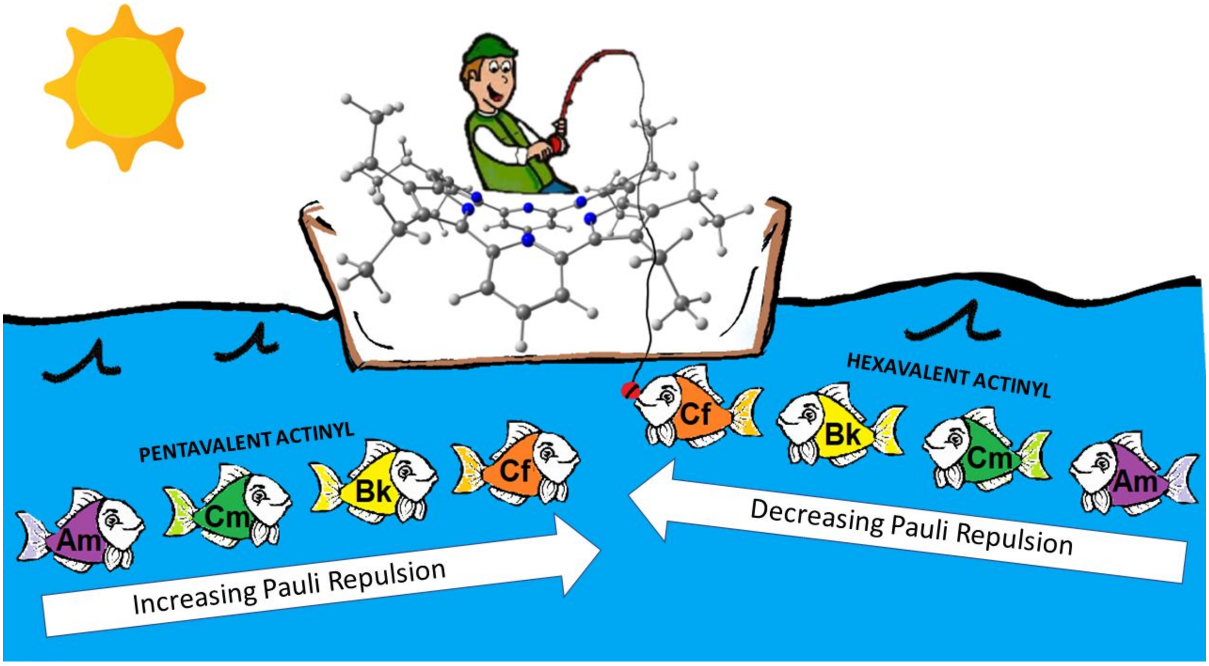

1. INTRODUCTION

The increased demand for low carbon fuel has shift our dependence to nuclear energy. This has accentuated the need to consider reprocessing concurrently generated spent nuclear fuel (SNF) which contains a significant number of radionuclides contributing to long-term radiation hazards.[1,2] These radionuclides include minor actinides (MAs) (Am, Cm, Bk and Cf) with long-term radioactivity ($t_{1/2}$=10^3-10^7 years)[3] and other fission products (U, Pu, Ln, Tc, Zr, etc.). In order to reduce the radiation hazards of SNF, the long-lived alpha-emitting MAs are converted into more stable elements by partitioning and transmutation processes, where the actinide/lanthanide (An/Ln) partitioning poses a significant challenge. This is attributed to the nearly common preference for the trivalent oxidation state (OS) (An^{3+}/Ln^{3+}) along with their similar ionic radii in aqueous solutions (as a result of the lanthanide/actinide contraction).[4–6] The small charge density difference between actinides and lanthanides proves insufficient amidst similar oxidation state and ionic radii and thereby limits the ability of chelating ligands for the An/Ln separation. However, the actinides are able to reach high OSs including +V and +VI while the lanthanides cannot exist in high OSs. Thus, the complexation of MAs from their dioxocation form in higher OSs is a topic of recent interest with potential applications in An/Ln separations. This study on MAs is relevant to the nuclear industry because of their unique structures and bonding in a ligand environment.[7–9]

While most stable higher OSs of the actinide (5f) series have been observed in early actinides, pentavalent and hexavalent actinyl cations ($[An^{V/VI}O_2]^{n+}$; n=1 and 2) for MAs (An=Am, Cm, Bk and Cf) have been reported to be stable in acid medium and/or complexing environment.[10–12] Burns *et al*. studied the oxidation of Am(III) to pentavalent americyl ($Am^{V}O_2^+$) and its stabilization in an acidic medium in the presence of hypochlorite.[13] Compared to the pentavalent OS, hexavalent americyl ($Am^{VI}O_2^+$) with a $5f^3$ occupied valence shell is energetically favoured[14] and more common.[15–19] Dau *et al.* recorded the first synthesis of bare Bk(V) and Cf(V) in their dioxide cation forms. They performed CCSD(T) calculations to show that linear actinyl(V) ions (AnO_2^+) are local energy minima structures through MdO_2^+ and all An from Pa through Es (except Cm) formed stable dioxide cations.[12] Kovacs *et al.* experimentally reported stable Cm(V) in a nitrate complex environment as $Cm^{V}O_2(NO_3)_2^-$ by electron donation from nitrate ligands along with $An^{V}O_2(NO_3)_2^-$ complexes of An = Pu, Am, Cm, Bk, and Cf. Based on computational analyses, across the series, a decrease in symmetry was observed, specifically the Cf complex showed a symmetry decrease from C_{2v} to C_2, along with increasing covalency.[20] Computational assessment of hexavalent curyl-crown ether complexes indicate the existence of OS +VI stabilized in an appropriate ligand environment.[21,22] In a recent study, based on computational assessment, Vasiliu *et al.* have reported that curyl (VI) and berkelyl (VI) could be stabilized in condensed phases by coordinating ligands based on their relative energies, while stabilization of californyl (VI) would be difficult even using strong donor ligands.[23] These studies demonstrate the significant impact of the ligand environment on oxidation state and stability of actinyl cations, especially for the minor actinides, relevant for the application in An/Ln partitioning. Relativistic effects play a vital role in the theoretical study of these heavy element complexes and are accounted for by the scalar relativistic and spin-orbit coupling (SOC) methods.[24]

Over the years, many macrocycles were studied for their potential to form complexes with actinide cations and for their chemo-sensing ability towards actinides.[25,26] The primary features of the macrocycles such as cavity size, oxidation state, conformational flexibility and basicity of donor atoms determine their feasibility to form complexes with actinides/actinyls. In addition to the commonly studied macrocyclic ligands (i.e., Schiff base macrocycles,[27–29] crown ethers,[30–34] calixarenes[35–37]), expanded porphyrins have been considered as potential complexing ligands for actinide/actinyl cations.[38–43] Apart from experimental studies, several reports of quantum chemical investigations on actinide/actinyl complexes with macrocyclic ligands aid in molecular tailoring of macrocyclic ligands with enhanced selectivity towards actinide/actinyl moieties.[44–49] However, most of these studies are limited to the early elements of the actinide series, while the minor actinides are less explored. The chemical richness of the ligands provides scope for different types of heterocycles to be fused with the expanded macrocycle (i.e., furan, thiophene, pyrrole and pyridine) resulting in modified electronic and steric properties. Over the past decades, Sessler's team has reported numerous stable expanded porphyrin-actinyl complexes,[50,51] including a stable uranyl-dipyriamethyrin complex.[52] The dipyriamethyrin ligand has been reported to form stable complexes with few actinyls and is the best-known pyridine-containing amethyrin analog.[53,54] We have recently reported the favorable bonding features between dipyriamethyrin and other AnO_2^{n+} (An

= Np, Pu and Am; *n* = 1,2) ions in gaseous and CH_2Cl_2 medium.[55] However, the understanding of the complexing ability of the dipyriamethyrin ligand with minor actinide as dioxocations remains unexplored.

In this study, a series of $[An^{V/VI}O_2(L)]^{1-/0}$ complexes (An = Am, Cm, Bk and Cf) have been studied using density functional theory (DFT) calculations. **Scheme 1** represents the neutral (LH_2) and deprotonated (L^{2-}) forms of the dipyriamethyrin ligand along with notations for the donor nitrogen atoms and the main carbon framework. The thermodynamic feasibility of the complexation reactions based on the geometries and electronic structures of bare actinyls and the ligand have been investigated. Further, the impact of the ligand environment on the hexavalent and pentavalent oxidation state of actinyls is explored while the various bonding analyses provide trends in observed properties among these dioxo forms of minor actinides in their bare and complexing environments.

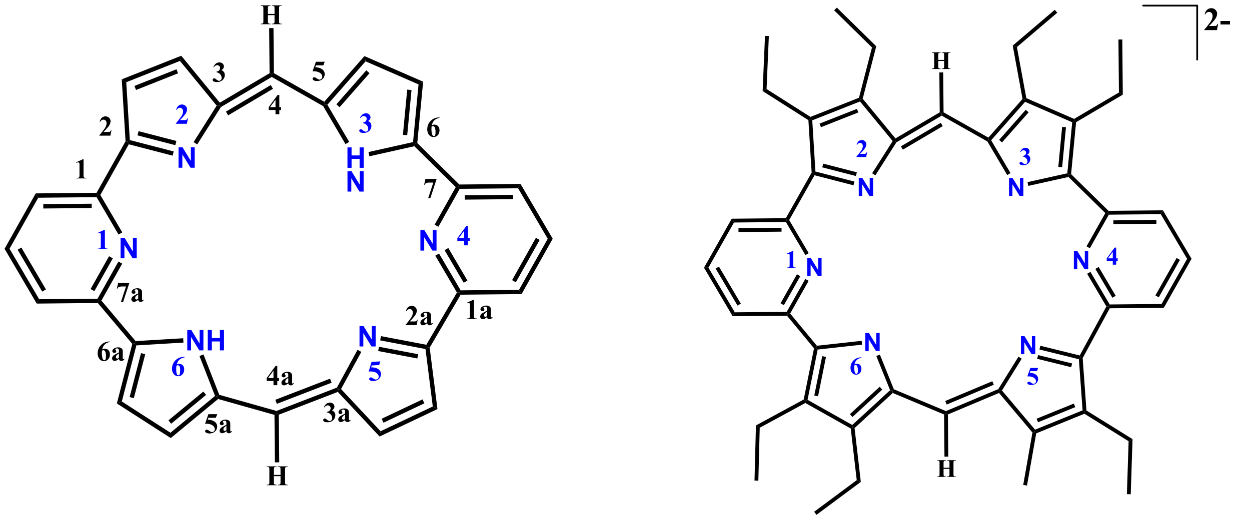

LH_2 **L^{2-}**

Scheme 1: The neutral (LH_2) and anionic (L^{2-}) forms of the dipyriamethyrin ligand with notations on nitrogen heteroatoms. All the alkyl chains in LH_2 are omitted for clarity.

2. COMPUTATIONAL DETAILS

The geometry optimization and vibrational frequency analysis of $[An^{V/VI}O_2(L)]^{1-/0}$ complexes (An = Am, Cm, Bk and Cf; and L = dipyriamethyrin ligand) and bare actinyl cations (AmO_2^{n+}, CmO_2^{n+}, BkO_2^{n+} and CfO_2^{n+}, n=1,2) were performed using DFT as implemented in the Amsterdam Modelling Suite (AMS) package, version Amsterdam Density Functional (ADF) 2019.305.[56,57] The generalized gradient approximation (GGA) PBE functional[58] along with Slater-type triple-ζ-plus-polarization (TZP) basis set[59–61] (GGA/PBE/TZP) was employed for all optimizations, analytical frequency, and electronic structure calculations. All positive frequencies obtained for the bare ligand, actinyl moieties, and their complexes indicate a local minimum on the potential energy surface and thus a low energy geometry. The unrestricted Kohn−Sham formalism was imposed on the calculations of open-shell actinyl complexes with high-spin states. The chosen functional and basis set have been proven to provide reasonable results for predicting geometries and electronic properties of 'actinide-macrocyclic ligand'-based complexes.[29,41,62–64] Scalar-relativistic corrections have been included using the Zero Order Regular Approximation (ZORA).[24,65–68] Along with the small-core ZORA basis sets, frozen-core approximations were used for all the atoms, where the core density is generated from a four-component Dirac-Slater calculation. The core orbitals 1s – 4f for An (An = Am, Cm, Bk, and Cf) and 1s for N, C, and O were frozen, while the remaining electrons were treated variationally. In order to verify the influence of the spin-orbit coupling, spin-orbit corrections (SOC) were computed for the formation energies and compared to those of the gas-phase optimized complexes. No symmetry constraints were imposed on complexes during the geometry optimizations. Convergence criteria and integration parameters of 10^{-6} au and 5.0, respectively, were applied to the self-consistent field (SCF) method.

The first reported actinyl- (i.e., uranyl-) dipyriamethyrin complex was synthesized in dichloromethane (CH_2Cl_2) solvent medium.[52] Hence, in addition to actinyl- binding which is the primary focus of this work, all actinyls and their complexes were also studied for solvent (CH_2Cl_2) effects on geometric and electronic properties using the conductor-like screening solvation model (COSMO).68,69,70 The atomic COSMO default radii as implemented in the ADF code were applied: An (Am, Cm, Bk, and Cf) 2.100 Å; C 1.700 Å; N 1.608 Å; O 1.517 Å; H 1.350 Å. The reaction energetics are reported as formation energy

(ΔE), free energy (ΔG), entropy (ΔS) and enthalpy (ΔH), with electronic energies combined with zero-point vibrational energy corrections.

Property calculations have been carried out to understand the influence of various factors that stabilize actinyl moieties in the hexavalent and pentavalent OSs within the ligand environment. The NBO 6.0 program implemented in the ADF 2019.305 software package was utilized to carry out the natural bond order (NBO) analyses which were performed based on the gas-phase optimized geometries of bare actinyl ions and their complexes.[71–73] The atomic charges of hetero donor atoms of ligands and actinyl ions in their bare and complex forms were computed using natural population analysis (NPA). These values tend to be stable because of the minimal basis set dependency exhibited by NPA. In order to understand the nature of bonding (i.e., ionic and covalent) and non-bonding interactions, the quantum theory of atoms in molecules (QTAIM) analysis was carried out. Actinyl cations are known to exhibit large SOC and multiconfigurational ground states. The SOC could be partly quenched upon equatorial ligand binding and mostly cancel in ligand exchange reactions (eq 2, as shown in section 3.3.4). This could introduce errors in electronic structure analyses; however, the influence of these errors should have less of an effect on the overall trend.[24,55] The relativistic effects of the independent fragments (i.e., actinyl and the ligand) and their complexes by both the scalar relativistic and SOC account for their electronic structure.[24] The bonding properties and stabilizing and destabilizing energy contributions associated with complexation reactions were further analyzed using the energy decomposition analysis (EDA)[74–76] and its extension extended transition state theory, combined with the natural orbitals for chemical valence theory[77] (ETS-NOCV) analysis, with the actinyl cation AnO_2^{n+} (n = 1, 2) as one fragment and the ligand dianion as the other, using single-point ADF calculations based on the PBE/TZP-optimized geometries in gas phase.

3. RESULTS AND DISCUSSION

3.1 Bare Actinyl Cations

The pentavalent and hexavalent actinyl cations of Am, Cm, Bk and Cf were considered for this study, with a focus on their stability and complexing ability. Based on previous literature[20,23], the reported high-spin states were considered as the stable ground states for these cations. The assumed spin states are in accordance with Hund's rule i.e., the stable ground state of ions is in the high-spin configuration. Thus, quintet and quartet for AmO_2^+ and AmO_2^{2+}; sextet and quintet for CmO_2^+ and CmO_2^{2+}; septet and sextet for BkO_2^+ and BkO_2^{2+}; octet and septet for CfO_2^+ and CfO_2^{2+}, respectively, were assigned as the stable ground states for geometry optimization and electronic structure calculations. The calculated bond lengths, bond angles, bond orders, NPA charges, spin densities, and vibrational stretching frequencies of the bare actinyl cations (gas phase) are tabulated in **Table S1**. For both $[An^{V/VI}O_2]^{1+/2+}$ the bond length between An and axial oxygens increases across the actinide series, i.e., from Am to Cf, which is contrary to the decreasing size of the actinide ions i.e., 1.04 to 1.01 Å due to the actinide contraction. This trend of increase in $An=O_{yl}$ bond lengths from Am onwards can be attributed to the relative energy[78] decrease and localization of the f orbitals with the increase in nuclear charge which is a phenomenon termed as the *plutonium turn*.[79] An inverse relation between bond length and bond order (both Mayer and NBO) for the actinyl cations is observed, except in the case of $Cf^VO_2^+$. The $O_{yl}(1)=An=O_{yl}(2)$ bond angles for all actinyl moieties is 180° indicating their linear structure, except for CfO_2^+ (94.9°) and CfO_2^{2+} (158.4°) which have bent structures. The formal septet spin state assigned to CfO_2^+ had optimized to a structure with a lower quintet spin state, with a higher spin density on O_{yl} (1.017 a.u.). This indicates a shift in excess spin density from metal to axial oxygens while increasing the $An=O_{yl}$ distance thereby lowering the metal OS, as the preference for higher oxidation states diminishes across the actinide series. A similar effect is seen in the CfO_2^{2+} moiety. The charge on An in pentavalent actinyl moieties increases from americyl to berkelyl and decreases in californyl, while in the hexavalent actinyl moieties there is a charge decrease from americyl to curyl and increases from berkelyl to californyl. This validates that An in pentavalent actinyl moieties will try to increase the charge to a stable (VI) OS, except in the case of californyl which tends toward a lower OS. On the other hand, the An atoms in the hexavalent moieties have charges around 2.158 a.u. close to the assigned (formal) +2 charge indicating a stable OS. Generally, shorter bond lengths yield higher frequencies for the corresponding stretching mode, and the same relation is observed here. This is known as a Badger's type relation between bond length and stretching frequency for high valent actinyls.[80,81] However, in CmO_2^+ a relatively low stretching frequency is observed, indicating a break in the trend around pentavalent curyl in its complex form. Overall, the hexavalent actinyl moieties show stronger bonds/interactions with oxygens compared to their pentavalent counterparts. It is evident that though Cf formally remains in its pentavalent and hexavalent form in californyl it shifts its spin density towards the oxygen atoms suggesting a preference for the lower OS. The bare dipyriamethyrin ligand has been previously studied computationally and its study here is beyond the scope of this paper.[53,55]

3.2 Geometry and Bonding Properties of Actinyl - Dipyriamethyrin Complexes

The geometric properties of $[\mathrm{Am^{V}O_2\text{-}L}]^{1-}$, $[\mathrm{Cm^{V}O_2\text{-}L}]^{1-}$, $[\mathrm{Bk^{V}O_2\text{-}L}]^{1-}$, $[\mathrm{Cf^{V}O_2\text{-}L}]^{1-}$, $[\mathrm{Am^{VI}O_2\text{-}L}]^{0}$, $[\mathrm{Cm^{VI}O_2\text{-}L}]^{0}$, $[\mathrm{Bk^{VI}O_2\text{-}L}]^{0}$, and $[\mathrm{Cf^{VI}O_2\text{-}L}]^{0}$ are discussed in this section. The ground electronic spin states of $\mathrm{Am^{5+}}$ (f^4), $\mathrm{Cm^{5+}}$ (f^5), $\mathrm{Bk^{5+}}$ (f^6), $\mathrm{Cf^{5+}}$ (f^7), $\mathrm{Am^{6+}}$ (f^3), $\mathrm{Cm^{6+}}$ (f^4), $\mathrm{Bk^{6+}}$ (f^5) and $\mathrm{Cf^{6+}}$ (f^6) in their complexes in accordance to Hund's rule, are the same as those of the stable high spin state of their corresponding actinyl fragments. Based on the verification in previous works,[27,31,53,55,60–62] the PBE functional was employed for calculations of structures and electronic properties of these theoretically designed macrocyclic complexes. The optimized geometries of the actinyl-dipyriamethyrin complexes are shown in **Figures 1** and **S1**. The geometric parameters based on the gas phase calculations are summarized in **Table S2**. Bond lengths are plotted as a graph in **Figure 2**. The optimized complexes show a distorted hexagonal bipyramidal geometry or a saddle-like structure, similar to the reported uranyl-dipyriamethyrin crystal structure.[52,53] The actinyl metal atom is located in the dipyriamethyrin ligand cavity with hexadentate coordination to six Lewis soft donor nitrogen atoms i.e., the nitrogen from 2 pyridine units and 4 pyrrole units of dipyriamethyrin. The actinyl moieties form axial bonds with dioxygen while the remaining bonds with the ligand are formed equatorially. The bond angles are observed to be similar in all complexes. The An-N1 and An-N4 bond lengths, in which N1 and N4 are pyridine nitrogen, are longer compared to those of the An-N2, An-N3, An-N5, and An-N6 bonds. This shows that the pyridine rings (N1/N4) make lesser contributions to the complexation than the pyrrole rings (N2/N5 and N3/N6). The values for these An-N bonds lengths suggest that their interactions could be ionic in nature. Among the $[\mathrm{An^{V}O_2\text{-}L}]^{1-}$ complexes there is a decrease in An-N bond lengths from $[\mathrm{Am^{V}O_2\text{-}L}]^{-1}$ to $[\mathrm{Bk^{V}O_2\text{-}L}]^{-1}$ and a steep decrease in $[\mathrm{Cf^{V}O_2\text{-}L}]^{1-}$, while the $\mathrm{An{=}O_{yl}}$ bond lengths increase from $[\mathrm{Am^{V}O_2\text{-}L}]^{1-}$ to $[\mathrm{Bk^{V}O_2\text{-}L}]^{1-}$ and decrease in $[\mathrm{Cf^{V}O_2\text{-}L}]^{1-}$. The decrease in bond lengths from $[\mathrm{Am^{V}O_2\text{-}L}]^{1-}$ to $[\mathrm{Cf^{V}O_2\text{-}L}]^{1-}$ is in accordance with the decrease in ionic radii due to actinides contraction. The increase in $\mathrm{An{=}O_{yl}}$ bond length follows the same trend as observed in the bare actinyl form, as discussed above, except that the decrease in An=O_{yl} bond length in $[Cf^{V}O_2\text{-}L]^{1-}$ may indicate that Cf could stabilize in the ligand environment probably in a lower OS than its assigned/formal pentavalent OS. This can be seen in its $[Cf^{V}O_2]^+$ form (see above) where it has a lower spin density than the rest of the actinyls indicating a possibility to shift towards a lower OS for stability. Among the $[An^{VI}O_2\text{-}L]^0$ complexes there is an increase in the An-L and An=O_{yl} bond lengths from $[Am^{VI}O_2\text{-}L]^0$ to $[Bk^{VI}O_2\text{-}L]^0$ and slight decreases in $[Cf^{VI}O_2\text{-}L]^0$. The increase in bond lengths may be due to the plutonium turn, however, the slight decrease in bond lengths of $[Cf^{VI}O_2\text{-}L]^0$ is negligible but may point to a random trend in structural properties in the succeeding heavier actinides owing to similar ionic radii generated by diminishing actinide contraction or else merely be an impact of charge effect. Comparison $[An^{V}O_2\text{-}L]^{1-}$ and $[An^{VI}O_2\text{-}L]^0$, the $[An^{VI}O_2\text{-}L]^0$ complexes show overall shorter An-L and An=O_{yl} bonds than their $[An^{V}O_2\text{-}L]^{1-}$ counterparts indicating that the hexavalent actinyl complexes form stronger ionic bonds than the pentavalent actinyl complexes. In addition to the gas phase geometry optimization, the structures were also optimized in solvent (CH_2Cl_2) medium using the implicit COSMO method to model the experimental environment. The bond lengths and bond angles for the COSMO optimized complexes are summarized in **Table S3**. From the table, we can see that the pentavalent actinyl-ligand complexes exhibit the same qualitative trends as the gas phase optimized geometries but with a slightly longer and shorter An-N bonds and An=O_{yl} bonds, respectively. Most actinyl complexes, based on literature, are identified with ionic/electrostatic interactions with the ligands and covalent interaction with the actinyl oxygens.[21,53] In the hexavalent actinyl-ligand complexes the An=O_{yl} bond lengths show a similar trend in a slightly higher magnitude to that of the pentavalent actinyl-ligand complexes while the An-N1/N4 bond lengths decrease from $[Am^{VI}O_2\text{-}L]^0$ to $[Bk^{VI}O_2\text{-}L]^0$ with a slight increase in $[Cf^{VI}O_2\text{-}L]^0$ and the remaining An-N bonds show a decrease in length from $[Am^{VI}O_2\text{-}L]^0$ to $[Cf^{VI}O_2\text{-}L]^0$.

3.2.1 BOND ORDERS

The bond order analysis gives insights into the nature of the bond in metal-ligand coordination complexes. Bond length and bond order generally show an inverse relationship, which fundamentally means that bonds with higher bond order are shorter bonds indicating stronger interactions in these complexes. **Table 1** shows the calculated NBO bond orders along with vibrational frequencies of all the complexes. Other calculated bond orders such as Mayer, Nalewajski-Mrozek, and Gophinatan-Jug bond orders are displayed in **Table S4**. In pentavalent actinyl complexes, the An=O$_{yl}$ bond orders decrease along with decreasing bond lengths from [Am^{V}O$_2$-L]$^{1-}$ to Bk^{V}O$_2$-L, which is due to the actinide contraction that was not observed in the bond lengths due to the plutonium turn. Thus, there isn't an inverse relationship between actinyl bond orders and bond lengths. The An-N bond orders increase from [Am^{V}O$_2$-L]$^{1-}$ to [Cf^{V}O$_2$-L]$^{1-}$, except in the case of [Cm^{V}O$_2$-L]$^{1-}$. The decrease in bond order in the [Cm^{V}O$_2$-L]$^{1-}$ complex is the actinide "break" point observed in trivalent actinides, which was reported by Yu and co-workers.[82] This was previously observed as a fluctuation in the trend of the vibrational frequencies of bare actinyl cations, specifically in Cm^{V}O$_2^{+}$, while the remaining cations displayed a badger-type relationship. This causes only a small overlap of the Cm 5f orbitals with the 2p orbitals of nitrogen, and no population decrease in 5f orbital populations accompanies this bond order decrease. The bond order rise beyond Cm is accounted for based on the population increase in 6d and 7s orbitals (see below, section 3.3.2). In the hexavalent complexes, bond orders decrease across the series in both An=O$_{yl}$ and An-N bonds, with a slight increase in An-N bond order for [Cf^{VI}O$_2$-L]^{0}. These bond orders are related to the bond length values given their inverse relationship. Overall, the [An^{VI}O$_2$-L]^{0} complexes show higher bond orders for An-N and An=O$_{yl}$ bonds as compared to their [An^{V}O$_2$-L]$^{1-}$ counterparts suggesting hexavalent actinyl complexes to have stronger bonds due to the additional electron that resides in the non-bonding or anti-bonding metal 5f orbital, respectively. The NBO bond order presents the following trend: An-N1/An-N4 < An-N2/N5 < An-N3/N6 in both [An$^{V/VI}$O$_2$-L]$^{1-/0}$ complexes. This trend is also consistent with the Mayer, Nalewajski-Mrozek, and Gophinatan-Jug bond orders (**Table S4**). The NBO bond order values are significantly lower than 1, with higher bond orders for the pyrrole nitrogen atoms compared to the pyridine nitrogen atoms, indicating stronger bonds for the former relative to the latter. The calculated NBO (0.153-0.365) and Mayer bond orders (0.118-0.218) lie in the range reported for ionic interactions.[29,30] The An=O$_{yl}$ bond orders (2.086 – 1.616) are significantly larger than for the An-L (0.153-0.365) bonds which confirms that actinyls have strong covalent bonds. This is in accordance with the overall trend in bond lengths. Generally, a higher bond order shows a higher vibrational frequency and this is also observed in [An^{VI}O$_2$-L]^{0} complexes; however, in [An^{V}O$_2$-L]$^{1-}$ complexes the charge effect affects this bond order-frequency relationship. Overall, $[An^{VI}O_2\text{-}L]^0$ show higher frequencies compared to $[An^{V}O_2\text{-}L]^{1-}$.

3.3 Electronic Properties of the Dipyriamethyrin - Actinyl (V and VI) Complexes

3.3.1 CHARGE ANALYSIS

The bonding environment and the impact of the ligand on the actinyl moieties in the complexes were investigated further based on their optimized geometries and charge analysis. The NPA charges were calculated to account for the charge distributions in the bare actinyl cation form and their respective complexes with dipyriamethyrin. The charges on coordinating atoms of the ligand and actinyl moieties are shown in **Figure 3** and the values are provided in **Tables S5** and **S6**. On complexation, there has been transfer of electronic density to An as the charges on An in its complexes are lower (less positive value) compared to those in bare actinyl $[AnO_2]^{1+/2+}$(V and VI) cations (more positive value). This indicates that the electron density flow was from the six donor nitrogen atoms of the ligand to the An (V/VI) metal center ($AnO_2^{+/2+}$), showing the possibility of Ligand to Metal Charge Transfer (LMCT) for complexation. The NPA charges show that An has a positive charge while the ligand's pyrrole and pyridine nitrogen atoms carry negative charges in all complexes. In $[An^{V}O_2\text{-}L]^{1-}$ complexes, the charge on An and O_{yl} increases from Am to Bk and significantly decreases in Cf^{V}. This could be due to the mentioned "plutonium turn" that is observed in actinides post plutonium where the f-orbital energies decrease and f-orbital localization increases which leads to larger charge transfer in Am to Bk. However, in Cf^{V} the plutonium turn is not observable because of the low charge on the bare $Cf^{V}O_2^+$ (1.867) moiety; this reflects as a relatively lower charge on Cf in $[Cf^{V}O_2\text{-}L]^{1-}$. In $[An^{VI}O_2\text{-}L]^0$ complexes, the charges on An increase from Am to Bk and decrease in Cf^{VI}; on the other hand, the charges on O_{yl} are observed to increase from Am to Cf. This demonstrates that the decrease in charge on Cf^{VI} indicates that the stabilization of Cf may occur in a lower OS. In all complexes, the charges on the pyrrole nitrogen atoms (N2, N3, N5, and N6) of the ligand contribute relatively more towards complexation than the pyridine nitrogen atoms (N1 and N4). This is evident from the higher charges on N1 and N4 which makes them more basic compared to the other nitrogen atoms of the pyrrole units. A similar behavior of the ligand was also observed on its complexation with the early actinyls (An=U-Am).[55] The axial oxygens (O_{yl}) of the actinyl in $[An^{V}O_2\text{-}L]^{1-}$ have significantly more negative charges than their $[An^{VI}O_2\text{-}L]^0$ counterparts which makes them more basic in nature. The trends observed in the charges correspond to those observed in the bond length and bond orders. The charges on the ligand nitrogen (negative values, from **Table S6**) are observed to slightly decrease (turning more negative, from **Table S5**) on complexation indicating the possibility of backdonation from the metal to the ligand.

3.3.2 ORBITAL POPULATION AND SPIN DENSITY

The valence orbitals for the actinide metal centers in their complexes and bare actinyl cation form are the 5f, 6d, 7s, and 7p orbitals for which the natural orbital populations have been calculated, **Tables S7** and **S8**. Based on the previous discussion, the bond formed between the metal and the ligand is due to the charges that transfer from the ligand to the actinyl center. This involves the orbital-overlap of 5f and 6d orbitals of An with 2p orbitals of N atoms of the ligand. From the orbital population analysis, it is evident that the 5f orbital occupation is higher than that of 6d and 7s orbitals in the An. The charges accepted by the metal mostly enter the 6d orbital where there is a small but steady increase in orbital population from $[\mathrm{Am}^{V/VI}O_2\text{-L}]^{1-/0}$ to $[\mathrm{Bk}^{V/VI}O_2\text{-L}]^{1-/0}$ and a slight decrease in $[\mathrm{Cf}^{V/VI}O_2\text{-L}]^{1-/0}$. The sudden decrease in charge on Cf, as discussed above, is reflected in the decrease in 6d and 7s population. It can be noticed that $[\mathrm{An}^{VI}O_2\text{-L}]^0$ complexes have a marginally lower 5f orbital population than their corresponding $[\mathrm{An}^{V}O_2\text{-L}]^{1-}$, however, the 6d and 7s orbital populations for $[\mathrm{An}^{VI}O_2\text{-L}]^0$ are relatively higher than for $[\mathrm{An}^{V}O_2\text{-L}]^{1-}$. This indicates that in $[\mathrm{An}^{VI}O_2\text{-L}]^0$ complexes the charges donated by the ligand prefer actinide 6d and 7s orbitals over 5f orbitals. In order to clearly understand the valence orbitals of An that are involved in complexation, it is necessary to understand the change in the orbital population of the actinide upon complexation. Comparing the orbital populations of An in bare actinyl and $[\mathrm{An}^{V/VI}O_2\text{-L}]^{1-/0}$ complexes, it is clear that the 6d orbitals are majorly involved in accepting the donated electrons from the ligand, not the 5f orbitals. In $[\mathrm{An}^{V}O_2\text{-L}]^{1-}$ complexes, the 5f orbital population changes upon complexation are: -0.15, -0.16, -0.17 and -0.11 for Am^{V}, Cm^{V}, Bk^{V} and Cf^{V}, respectively. In $[\mathrm{An}^{VI}O_2\text{-L}]^0$ complexes the 5f orbital population changes are -0.21, -0.04, -0.05, and -0.05, respectively, which is smaller compared to their pentavalent counterparts. The 6d and 7f orbital populations of An show a significant increase in the complex when compared to the bare actinyls. The increase is calculated to be around 0.54 to 0.18 for 6d orbitals and 0.14 to 0.17 for 7s orbitals, respectively. It is clear that the metal-to-ligand charge transfer is predominant in $[An^{VI}O_2\text{-}L]^0$ over $[An^{V}O_2\text{-}L]^{1-}$; where it is the 6d and 7s orbitals that determine the nature of ligand-metal orbital overlap and overall stability of the complexes.

The calculated spin densities on the An, O_{yl}, and donor nitrogen atoms of the ligand in the complexes are shown in **Table S9**. The natural electronic configurations of the actinide metals in the actinyl cation form and complex are displayed in **Tables S10** and **S11**. It is important to note that the nature of spin delocalization can be distinguished and explained by both experimental (e.g., Electron Paramagnetic Resonance (EPR) and Nuclear Magnetic Resonance (NMR)) and theoretical analyses. Aquino *et al.* used NMR shifts and scalar relativistic calculations to explain the spin-polarization mechanism in Ni and V metallocenes.[83] From **Table S9**, the spin density is concentrated on the f-orbital as expected for the actinyl in its bare and complexed forms. In $[Am^{V}O_2\text{-}L]^{1-}$, $[Cf^{V}O_2\text{-}L]^{1-}$, and $[Cf^{VI}O_2\text{-}L]^0$ complexes, the actual spin density is lower than the spin density in their respective bare actinyl form. This could be due to spin delocalization from the actinide to the ligand, indicating the possible backdonation from the actinide center, similar to the observations discussed under charges. In all the remaining complexes, the spin densities on An in their complexes are higher than their bare actinyl form; this is due to the spin delocalization from ligand to actinide. Sergentu *et al.* reported similar spin delocalization along with their mechanisms in 5f actinocene and 3d metallocenes.[84] We can infer from **Table S9** that, in $[Cf^{V}O_2\text{-}L]^{1-}$ and $[Cf^{VI}O_2\text{-}L]^0$ complexes, there is a significant lowering of the spin density, and the actual spin density is lower than the formal value because of backdonation of charges from Cf metal to ligand. In order to explain the unique property of Cf in its complexes, it is essential to assign the possible OS. Based on previous reports, the calculated spin density is an effective tool to deduce the OS.[23,85] In **Table S9**, based on the spin density and optimized geometry ($D_{\infty h}$), the OS for An has been assigned.[23] The extremely low spin density on Cf(VI) indicates that the Cf is not necessarily in the hexavalent state, rather, it is in a lower +V OS. It is known that heavier actinides are not stable in their high valent OS. This could be the reason for the unique properties exhibited by the nominally high-valent Cf (V/VI) that are, in fact, stabilized in a lower OS.

3.3.3 QUANTUM THEORY OF ATOMS IN MOLECULES (QTAIM)

The nature of various bonding and nonbonding interactions between metal and ligand in coordination complexes can be further characterized based on the partitioning of the electron density at zero flux surfaces using Bader's QTAIM analysis.[42,53,86,87] The QTAIM topology is labeled with descriptors such as electron density (ρ_c), Laplacian of electron density (∇^2 p_c), and energy density (H_c) at the bond critical points (BCPs) which provides information on the nature of bonding and non-bonding interactions. The electron density at the BCP provides a quantitative basis to define the nature of the interaction as the buildup of charges between the atoms measures the extent of overlap between the interacting orbitals. The characteristic covalent and ionic interactions have values of ρ_c > 0.2 e/bohr^3 and ρ_c < 0.1 e/bohr^3, respectively.[42,53,88] The electron density at BCPs of the actinyl-ligand complexes was calculated in the gas phase and tabulated in **Table S12**. Pictures of the QTAIM molecular topology are shown in **Figures 1** and **S2**. Based on the calculated ρ_c values it is evident that the actinyl-ligand bonds i.e., An-N bonds, are ionic while the An=O$_{yl}$ bonds are covalent in nature. The low electron density values at the BCPs of An-N1/An-N4 complements the analysis of bond lengths and charges which indicates their relatively lower involvement in bonding. On the other hand, ρ_c is highest for An-N2/An-N5 followed by An-N3/An-N6, which shows that the metal orbitals have maximum overlap with N2 and N5. Overall, An^{V}O$_2$-L and An^{VI}O$_2$-L complexes show approximately 2.63%, 3.22%, and 3.19% increase in electron density at the BCP of An-N1/N4, An-N2/N5, and An-N3/N6, respectively. In correspondence to bond lengths, bond orders and charges, the nitrogens of the pyrrole units (N2/5 and N3/N6) contribute more towards the complex formation with actinyl compared to the pyridine nitrogens (N1/N4). In the An^{V}O$_2$-L complexes, the ρ_c values increase going from Am to Cf, with a negligible "break" point in Cm that is seen in the An-N2/N5 and An-N3/N6 bonds but not in the An-N1/N4 bonds. The "break" point at Cm(V) is similar to the one observed from its bond orders. This indicates that the charge contributions are increasingly concentrated in the BCP to stabilize the pentavalent actinyl. On the other hand, a decrease in the ρ_c values along the series is observed in the An^{VI}O$_2$-L complexes, which indicates that the charge is localized on the metal rather than in the center of the overlapping orbitals. This observation is complementary to the earlier discussion of the charges that are seen on the nitrogen heteroatoms of the ligand and the metal. In all complexes other than those of Am, a non-bonded interaction is observed between the adjacent pyrrole nitrogen atoms i.e., the N3/N6 and N2/N5 atoms of the dipyriamethyrin ligand. This could be due to the stabilization of the dipyriamethyrin fragment upon the loss of two protons before complexing with the metal.

3.4. Thermodynamic Stability of Complexes and Spin-Orbit Corrections

The thermodynamic parameters provide insights into the feasibility of the complexation reaction which is presented as an experimental model to guide the synthesis. It is essential to adopt a practical model that would closely resemble the synthetic route yet is still simple enough to be amenable to quantum-chemical study at an appropriate level of theory. Following previous reports[43,89] we have utilized eq. 1, to analyze the feasibility of complex formation in its simplest form, ignoring the solvation effects that tend to affect particularly the bare actinyl ions.

$$AnO_2^{n+} + L^{2-} \rightarrow AnO_2L^{(n-2)} \; (n=1,2) \qquad (1)$$

The actinyl-ligand complex formation energy was computed in the gas phase and is shown in **Table 2**. Not surprisingly for a reaction that combines two gas-phase fragments of opposite charge, the energies of eq. (1) are large and negative., and the energies for the 2+ actinyl charge (n=2, An^{VI}) are approximately twice those of An^{V} (n=1). The most negative formation energy reflects the strongest binding strength of the actinyl with the ligand. The formation energies for $[An^{V}O_2\text{-}L]^{1-}$ complexes increase from Am to Bk and slightly decrease at Cf. A similar trend was observed in the charge, spin, and orbital population analyses of $[An^{V}O_2\text{-}L]^{1-}$ complexes. This verifies increased stability of these complexes across the period from Am to Bk. The exception for Cf may be due to its stabilization in the complex at a lower +IV OS. In the $An^{VI}O_2$-L complexes, the following trend is observed in its formation energies: $[Cf^{VI}O_2\text{-}L]^0 > [Am^{VI}O_2\text{-}L]^0 > [Bk^{VI}O_2\text{-}L]^0 > [Cm^{VI}O_2\text{-}L]^0$. The lowest formation energy of $[Cm^{VI}O_2\text{-}L]^0$ can be closely related to the "break" point observed in the bond orders, where a sudden decrease in bond order was observed at Cm. The lowered charge and spin density on Cf (VI) can be attributed to its higher formation energy.

In an experimental setup, the actinyl cation exists as a neutral fragment given the effect of the solvent it is present in. The synthesis of the uranyl-dipyriamethyrin complex[52] was carried out in an anaerobic environment with dry CH_2Cl_2. Thus, computing the formation energies of these complexes in solution according to eq. 1 would mean that we completely neglect the experimental factors that govern the complex formation. Various other parameters like counterion effects, solvation effects, and competing reactions are essential in determining the formation energy. Particularly, the ligand as a dianion after deprotonation would be able to react with both the actinyl as well as other protons. It is essential to use a model reaction that includes a product where the free protons released from the ligand are contained in bound form. Here, we have considered the dichlorinated forms of the actinyl ions $[An^{V}O_2\text{-}Cl_2]^{1-}$ and $[An^{VI}O_2\text{-}Cl_2]^{0}$, which are experimentally available forms of actinyls. The $[An^{V}O_2\text{-}Cl_2]^{1-}$ and $[An^{VI}O_2\text{-}Cl_2]^{0}$ were subject to geometry optimization in a continuum (COSMO) solvation environment. Their structural parameters have been tabulated in **Table S13** and the optimized geometries are shown in **Figure S3**. Both, the O=An=O and Cl-An-Cl bond angles decrease from linearity (179.9° to 92.9° and 90.4° to 177.4°). It is essential to note that the $[Cf^{VI/V}O_2Cl_2]^{0/1-}$ structures are extremely bent due to the stabilization of Cf in a lower oxidation state in its dichlorinated actinyl form. A similar bent structure was observed in $[Cf^{V/VI}O_2]^{+1/+2}$ with a lower spin density. Further, the $An{=}O_{yl}$ bond lengths increase on moving from Am to Cf. The $An{=}O_{yl}$ bond lengths are in the range of 1.8-1.9 Å and the An-Cl bond lengths are in the range of 2.7-2.5 Å for $[An^{V/VI}O_2\text{-}Cl_2]^{1-/0}$ moieties. The $An{=}O_{yl}$ bonds are elongated by about 0.1 Å on addition of the Cl units. Based on this discussion, the formation of the actinyl - dipyriamethyrin complex in CH_2Cl_2 solvent medium is represented as:

$$AnO_2Cl_2^{n-} + LH_2 \rightarrow AnO_2L^{n-} + 2\ HCl\ (n=0,1) \qquad (2)$$

The formation energies (ΔE) were calculated based on eq. (2) along with free energy (ΔG), enthalpy (ΔH) and entropy (ΔS). Calculated energy values for both gas phase and COSMO solvation are provided in **Table 2**. All entropy values are positive. $[An^{VI}O_2\text{-}L]^{0}$ complexes show negative ΔE, ΔG, and ΔH values in gas phase. In solvent medium, ΔE and ΔH are positive for $[Am^{VI}O_2\text{-}L]^{0}$ and $[Cm^{VI}O_2\text{-}L]^{0}$, while $[Am^{VI}O_2\text{-}L]^{0}$ has a positive ΔG and $[Cm^{VI}O_2\text{-}L]^{0}$ has a negative ΔG. $[Bk^{VI}O_2\text{-}L]^{0}$ and $[Cf^{VI}O_2\text{-}L]^{0}$ show positive ΔE, ΔG, and ΔH values. The most spontaneous and feasible thermodynamic parameters align with that of the $[Cf^{VI}O_2\text{-}L]^{0}$ complex. This can validate the suggested lower (+V) OS for the $[Cf^{VI}O_2\text{-}L]^{0}$ complex. All the other complexes show spontaneity at high temperatures. The $[An^{V}O_2\text{-}L]^{1-}$ complexes have positive ΔE, ΔG, and ΔH values which indicate that these complexes are formed by a spontaneous reaction that occurs spontaneously at high temperatures. In solution, i.e. eq. (2), the formation energy values are higher than those in eq. (1). It is important to note that in the solvent medium the $Cf^{VI}O_2\text{-}L$ complex shows higher negative ΔE, ΔG, and ΔH values and the lowest ΔS value. This could be attributed to the solvation effects that determine the energetics of both the reactants, specifically the $[Cf^{VI}O_2Cl_2]^{0}$, and the products. On comparing the thermodynamic properties of $An^{V}O_2$-L complexes in the gas and solvent phase, it is evident that the formation of these complexes will require high temperatures, especially even higher temperatures when considered in a solvent medium. On the other hand, formation of $[An^{VI}O_2\text{-L}]^0$ complexes in the gas phase is spontaneous, though requiring external heat for complex formation in a solvent medium. Overall, the formation of $[An^{VI}O_2\text{-L}]^0$ complexes is more feasible, especially the $[Cf^{VI}O_2\text{-L}]^0$ complex. This shows that the hexavalent actinyl based complexes are comparatively more stable than their pentavalent counterparts.

The formation energies (ΔE) of the complexes are compared with their values obtained with SOC. The scalar and SOC values of the ΔE of $[An^{V/VI}O_2\text{-L}]^{1-/0}$ are tabulated in **Table S14**. With respect to eq. 1, the SOC lowers the ΔE values for all $[An^{V}O_2\text{-L}]^{1-}$ complexes and the maximum lowering is seen for the $[Cf^{V}O_2\text{-L}]^{1-}$ complex. However, in $[An^{VI}O_2\text{-L}]^0$ complexes, SOC imposed ΔE values are higher than ΔE (scalar) values, except in the case of $[Cm^{VI}O_2\text{-L}]^0$. With respect to eq. 2 in the solvent medium, SOC shows lowered ΔE values, except in the case of $[Cf^{VI}O_2\text{-L}]^0$, where there is a higher value of ΔE with SOC. The SOC ΔE values in gas and solvent medium show the same trend with respect to reaction feasibility, with marginal differences in magnitude. With this insight, the following EDA calculations were carried out only in the gas phase to conserve computational resources and to limit redundant conclusions.

3.5 EDA/ETS-NOCV ANALYSIS

The optimized geometries of the complexes are used for the Energy Decomposition Analysis (EDA) along with extended transition state-natural orbitals for chemical valence (ETS-NOCV) analysis. These analyses are employed to quantitatively analyze the stabilizing and destabilizing energy contributions towards the formation of An-L chemical bonds in the complexation reaction. The actinyl cation and ligand anion were considered as the two fragments for complexation,[21,55,62,88] among other plausible fragment schemes.[90] From the charge analysis and spin density (sections 3.3.1, 3.3.2), the charge transfer and spin delocalization were observed from dipyriamethyrin to the actinyl along with some backdonation; this provides the basis for the choice of fragments. The calculated EDA results are shown in **Table S15** and **Figure 4**. The attractive interactions between the fragments are majorly from the electrostatic contributions ($\Delta E_{el\text{-}static}$) compared to the covalent orbital contributions (ΔE_{orb}) for all complexes. This confirms that the complexes are mostly ionic in nature.[91,92] The $[An^{VI}O_2\text{-}L]^{1-}$ complexes show higher binding energy compared to the pentavalent counterparts, due to the difference in charge. The repulsive Pauli energy and the attractive electrostatic contributions decrease as the covalent orbital interactions increase on going from Am to Cf in $[An^{VI}O_2\text{-}L]^0$ complexes. In the $[An^{V}O_2\text{-}L]^{1-}$ complexes, the Pauli energy and orbital contributions are seen to increase while electrostatic contributions decrease along the series. In both series, electrostatic and orbital contributions decrease from Am to Cf. However, the Pauli energy increases from Am to Cf in the case of the $[An^{V}O_2\text{-}L]^{1-}$ complexes, while it is seen to decrease from Am to Cf in $[An^{VI}O_2\text{-}L]^0$ complexes. This opposite trend seen in the repulsive Pauli energy contribution favors the higher relative stability of the $[An^{VI}O_2\text{-}L]^0$ complexes along with high steric and orbital energy contributions, though the magnitude of the Pauli energy is close for Cf (83.18/85.31 kcal/mol) in both its complexes. The total interaction energy (ΔE_{int}) increases along with the increase in orbital contributions, which indicates that the orbital covalency supports the interaction in the heavier actinyl complexes. In all of these parameters, the Cf complexes show deviations because of the metal to ligand backdonation and lower actual spin compared to the formal value. The increase in orbital energy from Am to Cf, and Cf complexes having the maximum orbital contributions, clearly shows that the 5f orbital localization has set in and 6d and 7s orbital involvement has begun to increase. This is also reflected in the orbital population and thus the overall interaction energy is brought about by an increased number of orbitals (i.e., 5f, 6d, and 7s) that overlap with the 2p orbitals of the ligand nitrogen atoms, thus, increasing the covalent character of the complexes.

The covalent character of the An-L bonds is validated by the ETS-NOCV analysis using the contour plots as shown in **Table S16**. The alpha and beta orbital contributions together account for the ΔE_{orb} value. Both, σ and π type overlap within the An-N bonds are observed from the contour plots. The σ orbital overlap is mainly between the 2p orbital of the ligand and the 6d/5f orbitals of the metal, along with other π orbital overlap. The (ΔE_i^{orb}) energetic stabilization energy contributions differ between the complexes, **Table S16**. The $[An^{VI}O_2\text{-}L]^0$ complexes show energetic stabilization higher than their pentavalent counterparts. This indicates that the ligand affinity is more towards hexavalent than pentavalent actinyl complexes. As seen in the EDA, the Cf complexes show orbital-driven covalency, and this is evident from the dominant NOCV contour plots showing σ orbital overlap. It is also seen that metal to ligand backdonation plays a significant role to stabilize the Cf complexes.

3.6 MOLECULAR ORBITAL ANALYSIS

Molecular orbital analysis was carried out to further understand the contributing or stabilizing valence orbitals in the complex. The occupied MOs stabilizing the complex are shown in **Figure 5** and **Figure S4**. From these figures, it is seen that 5f (specifically, f_{z^3}, f_{xz^2}, f_{yz^2}, f_{xyz}, and $f_{z(x^2-3y^2)}$) and 6d orbitals (in particular, d_{z^2}, d_{xy}, and $d_{x^2-y^2}$) are the major contributing orbitals that bond with the 2p (i.e., $2p_x$ and $2p_y$) orbitals of the pyridine and pyrrole nitrogen atoms in the ligand. The actinide contraction matches the 5f energy levels of the actinide with the 2p orbitals of the ligands more than the 6d orbitals, however, the involvement of the An 6d in bonding also increases because of the radial distribution that is less contracted. This complements the results of the ETS-NOCV analysis. The increasing effect of the 6d involvement in the bonding may be induced by the f-orbital localization, as beyond Am towards heavier actinides the plutonium turn affects the nature of bonding interactions. The greater number of contributing MOs to the donor-acceptor interactions indicates the stability of the complex.[52,53,55] The number of contributing MOs increases from Am<Cm<Bk<Cf in both $[An^{V/VI}O_2\text{-}L]^{1-/0}$ complexes. The HOMO-LUMO gap (shown in **Figure S5**) in hexavalent complexes is smaller than that in pentavalent complexes, except in the case of $[Am^{VI}O_2\text{-}L]^0$. In the $[An^{VI}O_2\text{-}L]^0$ complexes, the HOMO-LUMO gap decreases from Am>Cf>Bk>Cm along which the actinyl fragment to ligand backdonation becoming a prominent effect. This backdonation is the significant stabilizing factor in $[Cf^{V/VI}O_2\text{-}L]^{1-/0}$ complexes.

4. Conclusion

Numerous reported explorations to understand the complexation of high valent early actinides in their dioxo form with macrocyclic ligands have left a gap in research for similar understanding of the minor actinides. In this work, we have employed scalar relativistic DFT to analyze the complex formation between the $[An^{V/VI}O_2]^{n+}$, where An=Am, Cm, Bk, and Cf; n=1,2, and the dipyriamethyrin ligand, and report the unique trends in the bonding properties. The structural, bonding, and electronic properties have been analyzed for the actinyl-ligand complex formation. The bonding environment is explored based on the bond lengths and bond orders, such as Mayer and NBO; this was further quantitatively understood based on EDA/ETS-NOCV and MO analyses, and trends in the bonding nature along the actinide series were observed. Generally, N1 and N4, i.e., pyrrole nitrogen atoms, show longer bond lengths and smaller bond orders compared to N2/N5 and N5/N6, i.e., pyridine nitrogen atoms. The An=O_{yl} bonds are significantly shorter than the An-N bonds. A similar effect is observed in the charges where more charge depletion is seen on the pyrrole nitrogen atoms compared to the pyridine nitrogen atoms. This makes the pyrrole nitrogen significant contributors to the complexation. The formation of the complex is mostly due to ligand to metal charge transfer (LMCT), as the spin density is concentrated on the metal center. The lowest spin density on the Cf(VI) indicates that it may not exist in the formal OS but rather in a lower (+V) OS. The orbital population shows increasing involvement along the series of 5f and 6d orbitals of the actinyl in overlap with 2p of the ligand nitrogens. The affinity towards complex formation follows the order $[Cf^{VI}O_2\text{-}L]^0 > [Am^{VI}O_2\text{-}L]^0 > [Bk^{VI}O_2\text{-}L]^0 > [Cm^{VI}O_2\text{-}L]^0 > [Bk^{V}O_2\text{-}L]^{1-} > [Cf^{V}O_2\text{-}L]^{1-} > [Cm^{V}O_2\text{-}L]^{1-} > [Am^{V}O_2\text{-}L]^{1-}$ (eq. 1). In the solvent medium, the $[Cf^{VI}O_2\text{-}L]^0$ complex shows spontaneous reaction feasibility while all other complexes are spontaneous at higher temperatures, as the reaction is endothermic at standard conditions. The overall trends in thermodynamic feasibly are similar upon including SOC. EDA analysis indicates that the major attractive contributions are from the electrostatic energy which decreases on going from Am to Cf. However, increase in the covalent orbital contributions from Am to Cf strongly influences the total interaction energy for hexavalent complexes. The ETS-NOCV and MO analyses show the flow of electrons through σ donation from 5f/6d of actinyl to 2p orbitals of N atoms in the ligand. The HOMO-LUMO gap also suggests backdonation from metal to ligand which increases from Am to Cf. A greater number of HOMOs in the Cf complexes tend to contribute to the stabilization of the donor-acceptor interaction. Overall, the energetics and bond parameters suggest that $[An^{VI}O_2\text{-}L]^0$ complexes have stronger binding ability as indicated by the total interaction energy (along with increasing orbital energy contributions) and shorter bonds than $[An^{V}O_2\text{-}L]^{1-}$. The stability of the complexes increases from Am to Cf; the low spin density on Cf on bonding with ligand and backdonation from californyl to dipyriamethyrin ligand was observed.

ACKNOWLEDGEMENTS

AJG acknowledges the SRMIST fellowship for pursuing the research. GS acknowledges funding from the Natural Sciences and Engineering Research Council of Canada (NSERC; Discovery Grant) and the Center for Actinide Science and Technology, an Energy Frontier Research Center funded by the U.S. Department of Energy, Office of Science, Basic Energy Sciences (DOE BES) under Award Number DE-SC0016568. Y.G would like to thank the support of the National Science Foundation of China under grant Nos. 11904049. Y.G. further acknowledges the assistance of the China Postdoctoral Science Foundation (2019M653365) and the scholarships from the China Scholarship Council (CSC).

SUPPORTING INFORMATION

The supporting information contains bond parameters, NPA charges, natural orbital population and spin density of bare actinyl cations, ligand anions and their complexes. QTAIM topology, NOCV contour plots, molecular orbitals and HOMO-LUMO energy gaps are presented as figures in the supporting information.

REFERENCES

1 E. Kintisch, *Science (1979)*, 2005, **310**, 1406–1406.

2 P. S. Roger Cashmore, Jonathan Billowes, Wyn Bowen, Christine Brown, Robin Grimes, Roger Howsley, Francis Livens, John Simpson, *The Royal Society Science Policy Centre report 10/11*, 2011, 1–79.

3 Z. Yoshida, S. G. Johnson, T. Kimura and J. R. Krsul, *The Chemistry of the Actinide and Transactinide Elements*, 2007, 699–812.

4 S. A. Ansari, P. Pathak, P. K. Mohapatra and V. K. Manchanda, *Separation & Purification Reviews*, 2011, **40**, 43–76.

5 H. Yoshimochi, M. Nemoto, K. Mondo, S. Koyama And T. Namekawa, *Journal of Nuclear Science and Technology*, 2004, **41**, 850–856.

6 K. Morimoto, M. Kato, H. Uno, A. Hanari, T. Tamura, H. Sugata, T. Sunaoshi and S. Kono, *Journal of Physics and Chemistry of Solids*, 2005, **66**, 634–638.

7 J. P. Austin, M. Sundararajan, M. A. Vincent and I. H. Hillier, *Dalton Transactions*, 2009, 5902-5909.

8 L. S. Natrajan, *Coordination Chemistry Reviews*, 2012, **256**, 1583–1603.

9 Y. Wang, S.-X. Hu, L. Cheng, C. Liang, X. Yin, H. Zhang, A. Li, D. Sheng, J. Diwu, X. Wang, J. Li, Z. Chai and S. Wang, *CCS Chemistry*, 2020, **2**, 425–431.

10 C. Riddle, K. Czerwinski, E. Kim, P. Paviet, P. Weck, F. Poineau and S. Conradson, *Journal of Radioanalytical and Nuclear Chemistry*, 2016, **309**, 1087–1095.

11 C. den Auwer, E. Simoni, S. Conradson and C. Madic, *European Journal of Inorganic Chemistry*, 2003, **2003**, 3843–3859.

12 P. D. Dau, M. Vasiliu, K. A. Peterson and D. A. Dixon, *Chemistry - A European Journal*, 2017, **23**, 17369–17378.

13 J. D. Burns, T. C. Shehee, A. Clearfield and D. T. Hobbs, *Analytical Chemistry*, 2012, **84**, 6930–6932.

14 C. Riddle, K. Czerwinski, E. Kim, P. Paviet, P. Weck, F. Poineau and S. Conradson, *Journal of Radioanalytical and Nuclear Chemistry*, 2016, **309**, 1087–1095.

15 F. Weigel and G. Hoffmann, *Journal of the Less Common Metals*, 1976, **44**, 133–136.

16 J. S. Coleman, T. K. Keenan, L. H. Jones, W. T. Carnall and R. A. Penneman, *Inorganic Chemistry*, 1963, **2**, 58–61.

17 G. P. Horne, T. S. Grimes, W. F. Bauer, C. J. Dares, S. M. Pimblott, S. P. Mezyk and B. J. Mincher, *Inorganic Chemistry*, 2019, **58**, 8551–8559.

18 T. K. Keenan, *Inorganic and Nuclear Chemistry Letters*, 1968, **4**, 381–384.

19 L. B. Asprey, S. E. Stephanou and R. A. Penneman, *J Am Chem Soc*, 1951, **73**, 5715–5717.

20 A. Kovács, P. D. Dau, J. Marçalo and J. K. Gibson, *Inorganic Chemistry*, 2018, **57**, 9453–9467.

21 S.-X. Hu, W.-L. Li, L. Dong, J. K. Gibson and J. Li, *Dalton Transactions*, 2017, **46**, 12354–12363.

22 P. Zhang, Y.-X. Wang, P. Zhang, S.-A. Wang and S.-X. Hu, *Inorganic Chemistry*, 2020, **59**, 11953–11961.

23 M. Vasiliu, T. Jian, J. K. Gibson, K. A. Peterson and D. A. Dixon, *Inorganic Chemistry*, 2020, **59**, 4554–4566.

24 J. Autschbach, in *Quantum Theory for Chemical Applications*, Oxford University Press, 2020, pp. 555–592.

25 V. Alexander, *Chemical Reviews*, 1995, **95**, 273–342.

26 B. M. Rambo and J. L. Sessler, *Chemistry - A European Journal*, 2011, **17**, 4946–4959.

27 X.-J. Zheng, N. L. Bell, C. J. Stevens, Y.-X. Zhong, G. Schreckenbach, P. L. Arnold, J. B. Love and Q.-J. Pan, *Dalton Transactions*, 2016, **45**, 15910–15921.

28 Q.-J. Pan, G. Schreckenbach, P. L. Arnold and J. B. Love, *Chemical Communications*, 2011, **47**, 5720.

29 G. A. Shamov and G. Schreckenbach, *The Journal of Physical Chemistry A*, 2006, **110**, 9486–9499.

30 P. Zhang, Y.-X. Wang, P. Zhang, S.-A. Wang and S.-X. Hu, *Inorganic Chemistry*, 2020, **59**, 11953–11961.

31 S.-X. Hu, J.-J. Liu, J. K. Gibson and J. Li, *Inorganic Chemistry*, 2018, **57**, 2899–2907.

32 S.-X. Hu, W.-L. Li, L. Dong, J. K. Gibson and J. Li, *Dalton Transactions*, 2017, **46**, 12354–12363.

33 G. A. Shamov, G. Schreckenbach, R. L. Martin and P. J. Hay, *Inorganic Chemistry*, 2008, **47**, 1465–1475.

34 D. L. Clark, D. W. Keogh, P. D. Palmer, B. L. Scott and C. D. Tait, *Angewandte Chemie International Edition*, 1998, **37**, 164–166.

35 B. Mokhtari, K. Pourabdollah and N. Dallali, *Journal of Radioanalytical and Nuclear Chemistry*, 2011, **287**, 921–934.

36 P. K. Mohapatra, A. Sengupta, M. Iqbal, J. Huskens, S. v. Godbole and W. Verboom, *Dalton Transactions*, 2013, **42**, 8558.

37 K. Kiegiel, L. Steczek and G. Zakrzewska-Trznadel, *Journal of Chemistry*, 2013, **2013**, 1–16.

38 A. Alka, V. S. Shetti and M. Ravikanth, *Coordination Chemistry Reviews*, 2019, **401**, 213063.

39 J. T. Brewster, H. Zafar, H. D. Root, G. D. Thiabaud and J. L. Sessler, *Inorganic Chemistry*, 2020, **59**, 32–47.

40 J. L. Sessler, D. Seidel, A. E. Vivian, V. Lynch, B. L. Scott and D. W. Keogh, *Angewandte Chemie*, 2001, **113**, 611–614.

41 G. A. Shamov, *J Am Chem Soc*, 2011, **133**, 4316–4329.

42 M. Yang, W. Ding and D. Wang, *New Journal of Chemistry*, 2017, **41**, 63–74.

43 M.-S. Liao, T. Kar and S. Scheiner, *The Journal of Physical Chemistry A*, 2004, **108**, 3056–3063.

44 J.-H. Lan, C.-Z. Wang, Q.-Y. Wu, S.-A. Wang, Y.-X. Feng, Y.-L. Zhao, Z.-F. Chai and W.-Q. Shi, *The Journal of Physical Chemistry A*, 2015, **119**, 9178–9188.

45 M. B. Jones and A. J. Gaunt, *Chemical Reviews*, 2013, **113**, 1137–1198.

46 D.-C. Sergentu, T. J. Duignan and J. Autschbach, *The Journal of Physical Chemistry Letters*, 2018, **9**, 5583–5591.

47 C. Xu, G. Tian, S. J. Teat, G. Liu and L. Rao, *Chemistry – A European Journal*, 2013, **19**, 16690–16698.

48 M. D. Ogden, S. I. Sinkov, G. J. Lumetta and K. L. Nash, *Journal of Solution Chemistry*, 2012, **41**, 616–629.

49 P. Zhang, Y.-X. Wang, P. Zhang, S.-A. Wang and S.-X. Hu, *Inorganic Chemistry*, 2020, **59**, 11953–11961.

50 V. v. Roznyatovskiy, C.-H. Lee and J. L. Sessler, *Chem. Soc. Rev.*, 2013, **42**, 1921–1933.

51 J. L. Sessler and D. Seidel, *Angewandte Chemie International Edition*, 2003, **42**, 5134–5175.

52 J. T. Brewster, Q. He, G. Anguera, M. D. Moore, X.-S. Ke, V. M. Lynch and J. L. Sessler, *Chemical Communications*, 2017, **53**, 4981–4984.

53 J. T. Brewster, D. N. Mangel, A. J. Gaunt, D. P. Saunders, H. Zafar, V. M. Lynch, M. A. Boreen, M. E. Garner, C. A. P. Goodwin, N. S. Settineri, J. Arnold and J. L. Sessler, *J Am Chem Soc*, 2019, **141**, 17867–17874.

54 J. T. Brewster, H. D. Root, D. Mangel, A. Samia, H. Zafar, A. C. Sedgwick, V. M. Lynch and J. L. Sessler, *Chemical Science*, 2019, **10**, 5596–5602.

55 E. Varathan, Y. Gao and G. Schreckenbach, *The Journal of Physical Chemistry A*, 2021, **125**, 920–932.

56 G. te Velde, F. M. Bickelhaupt, E. J. Baerends, C. Fonseca Guerra, S. J. A. van Gisbergen, J. G. Snijders and T. Ziegler, *Journal of Computational Chemistry*, 2001, **22**, 931–967.

57 A. L. Y. E.J. Baerends, T. Ziegler, A.J. Atkins, J. Autschbach, O. Baseggio, D. Bashford, A. Bérces, F.M. Bickelhaupt, C. Bo, P.M. Boerrigter, C. Cappelli, L. Cavallo, C. Daul, D.P. Chong, D.V. Chulhai, L. Deng, R.M. Dickson, J.M. Dieterich, F. Egidi, D.E. Ellis,.., A.L. Yakovlev, *AMS, ADF 2019.305, SCM*.

58 J. P. Perdew, K. Burke and M. Ernzerhof, *Physical Review Letters*, 1996, **77**, 3865–3868.

59 D. P. Chong, E. van Lenthe, S. van Gisbergen and E. J. Baerends, *Journal of Computational Chemistry*, 2004, **25**, 1030–1036.

60 D. P. Chong *, *Molecular Physics*, 2005, **103**, 749–761.

61 E. van Lenthe and E. J. Baerends, *Journal of Computational Chemistry*, 2003, **24**, 1142–1156.

62 G. A. Shamov and G. Schreckenbach, *Inorganic Chemistry*, 2008, **47**, 805–811.

63 G. A. Shamov and G. Schreckenbach, *The Journal of Physical Chemistry A*, 2005, **109**, 10961–10974.

64 G. A. Shamov and G. Schreckenbach, *The Journal of Physical Chemistry A*, 2006, **110**, 12072–12072.

65 E. van Lenthe, E. J. Baerends and J. G. Snijders, *The Journal of Chemical Physics*, 1993, **99**, 4597–4610.

66 E. van Lenthe, A. Ehlers and E.-J. Baerends, *The Journal of Chemical Physics*, 1999, **110**, 8943–8953.

67 E. van Lenthe, E. J. Baerends and J. G. Snijders, *The Journal of Chemical Physics*, 1994, **101**, 9783–9792.

68 E. van Lenthe, J. G. Snijders and E. J. Baerends, *The Journal of Chemical Physics*, 1996, **105**, 6505–6516.

69 C. C. Pye and T. Ziegler, *Theoretical Chemistry Accounts: Theory, Computation, and Modeling (Theoretica Chimica Acta)*, 1999, **101**, 396–408.

70 A. Klamt and G. Schüürmann, *J. Chem. Soc., Perkin Trans. 2*, 1993, 799–805.

71 A. E. Reed, R. B. Weinstock and F. Weinhold, *The Journal of Chemical Physics*, 1985, **83**, 735–746.

72 A. E. Reed, L. A. Curtiss and F. Weinhold, *Chemical Reviews*, 1988, **88**, 899–926.

73 E. D. Glendening, J. K. Badenhoop, A. E. Reed, J. E. Carpenter, J. A. Bohmann, C. M. Morales, C. R. Landis and F. Weinhold, 2001.

74 T. Ziegler and A. Rauk, *Inorganic Chemistry*, 1979, **18**, 1558–1565.

75 T. Ziegler and A. Rauk, *Theoretica Chimica Acta*, 1977, **46**, 1–10.

76 K. Morokuma and K. Kitaura, in *Chemical Applications of Atomic and Molecular Electrostatic Potentials*, Springer US, Boston, MA, 1981, pp. 215–242.

77 A. Michalak, M. Mitoraj and T. Ziegler, *The Journal of Physical Chemistry A*, 2008, **112**, 1933–1939.

78 S. T. Liddle, *Angewandte Chemie International Edition*, 2015, **54**, 8604–8641.

79 J.-B. Liu, G. P. Chen, W. Huang, D. L. Clark, W. H. E. Schwarz and J. Li, *Dalton Transactions*, 2017, **46**, 2542–2550.

80 J. Cioslowski, G. Liu and R. A. Mosquera Castro, *Chemical Physics Letters*, 2000, **331**, 497–501.

81 The Actinide Research Quarterly: 1st Quarter 2004, https://www.lanl.gov/orgs/nmt/nmtdo/AQarchive/04spring/correlation.html, (accessed December 9, 2021).

82 X. Yu, D.-C. Sergentu, R. Feng and J. Autschbach, *Inorganic Chemistry,* 2021, **60**, 17744–17757.

83 F. Aquino, B. Pritchard and J. Autschbach, *Journal of Chemical Theory and Computation*, 2012, **8**, 598–609.

84 D.-C. Sergentu, F. Gendron and J. Autschbach, *Chemical Science*, 2018, **9**, 6292–6306.

85 M. P. Kelley, G. J.-P. Deblonde, J. Su, C. H. Booth, R. J. Abergel, E. R. Batista and P. Yang, *Inorganic Chemistry*, 2018, **57**, 5352–5363.

86 R. F. W. Bader, *Accounts of Chemical Research*, 1985, **18**, 9–15.

87 R. F. W. Bader, *Chemical Reviews*, 1991, **91**, 893–928.

88 S. Chattaraj, A. Bhattacharyya and B. Sadhu, *Inorganic Chemistry*, 2021, **60**, 15351–15363.

89 Y. Gong and J. K. Gibson, *Inorganic Chemistry*, 2014, **53**, 5839–5844.

90 L. Bondì, A. L. Garden, P. Jerabek, F. Totti and S. Brooker, *Chemistry – A European Journal*, 2020, **26**, 13677–13685.

91 Y. Gao, E. Varathan, P. Grover and G. Schreckenbach, *Inorganic Chemistry*, 2021, **60**, 6971–6975.

92 Y. Gao, P. Grover and G. Schreckenbach, *Chemical Science*, 2021, **12**, 2655–2666.

TABLES & FIGURES

Table 1. NBO bond orders of the actinyl (V and VI) complexes and O=An=O stretching vibrational frequencies (cm^{-1})

	$Am^{V}O_2$-L^-	$Cm^{V}O_2$-L^-	$Bk^{V}O_2$-L^-	$Cf^{V}O_2$-L^-	$Am^{VI}O_2$-L	$Cm^{VI}O_2$-L	$Bk^{VI}O_2$-L	$Cf^{VI}O_2$-L
NBO Bond Orders								
An=O_{yl}(1)	1.980	1.764	1.616	1.600	2.086	1.858	1.629	1.616
An=O_{yl}(2)	1.989	1.777	1.628	1.614	2.097	1.837	1.641	1.626
An-N1	0.158	0.151	0.163	0.187	0.282	0.191	0.186	0.186
An-N2	0.209	0.200	0.212	0.214	0.362	0.264	0.235	0.239
An-N3	0.207	0.201	0.212	0.224	0.363	0.267	0.233	0.238
An-N4	0.158	0.155	0.162	0.199	0.282	0.197	0.183	0.186
An-N5	0.209	0.204	0.209	0.258	0.368	0.238	0.231	0.241
An-N6	0.207	0.199	0.209	0.260	0.363	0.233	0.233	0.240
Vibrational Frequency (cm^{-1})								
$\boldsymbol{\nu}_{symm}$ (AnO_2-L)	727.432	698.999	726.707	701.475	777.626	699.929	706.056	714.58
$\boldsymbol{\nu}_{asymm}$(AnO_2-L)	852.983	792.069	797.576	796.372	916.654	864.893	810.427	807.044

Table 2. Formation energy (ΔE), enthalpy (ΔH), Gibbs free Energies (ΔG) (kcal/mol) and entropy (ΔS) (cal/K.mol) at the PBE/TZP Level of Theory

	$Am^{V}O_2$-L^-	$Cm^{V}O_2$-L^-	$Bk^{V}O_2$-L^-	$Cf^{V}O_2$-L^-	$Am^{VI}O_2$-L	$Cm^{VI}O_2$-L	$Bk^{VI}O_2$-L	$Cf^{VI}O_2$-L
$\Delta E_{\text{eq1; gas}}$	-294.10	-302.8	-312.75	-304.78	-619.11	-595.93	-618.99	-641.04
$\Delta E_{\text{eq2; gas}}$	14.81	17.23	90.66	42.14	-15.24	-9.45	-13.21	-33.35
$\Delta H_{\text{eq2; gas}}$	8.29	10.98	83.33	34.63	-21.55	-14.91	-18.14	-38.52
$\Delta G_{\text{eq2; gas}}$	4.68	7.01	77.47	31.58	-24.17	-18.8	-24.18	-42.25
$\Delta S_{\text{eq2; gas}}$	12.64	13.89	19.25	10.80	9.321	13.52	20.76	10.80
$\Delta E_{\text{eq2; sol}}$	32.65	31.59	31.00	44.53	19.10	5.72	-6.47	-98.92
$\Delta H_{\text{eq2; sol}}$	27.14	26.20	25.70	38.07	14.55	0.12	-11.24	-105.50
$\Delta G_{\text{eq2; sol}}$	23.59	22.71	21.63	36.93	13.29	-3.82	-17.01	-108.95
$\Delta S_{\text{eq2; sol}}$	11.91	11.67	5.37	3.82	4.23	13.21	19.35	1.14

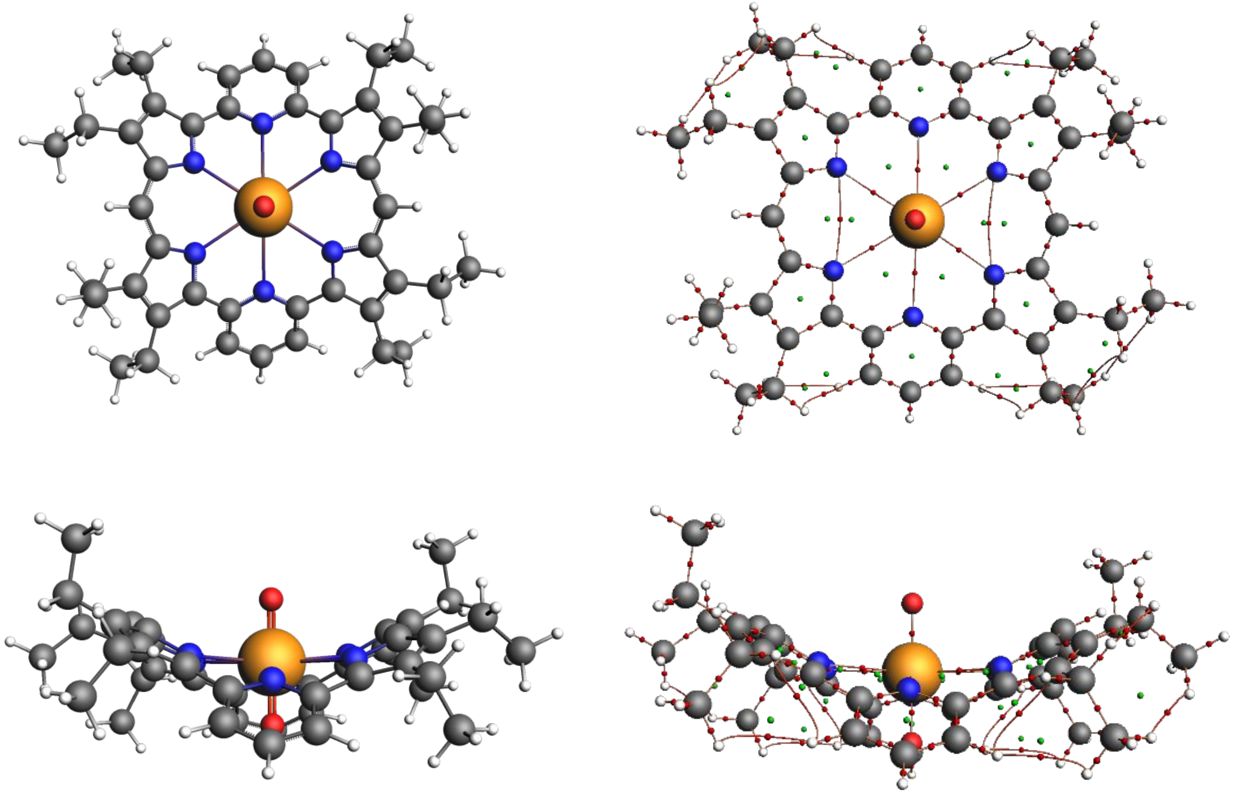

Figure 1. (Left top and bottom) Optimized geometry of $[Cf^{VI}O_2\text{-}L]^0$ complex, top and side view, optimized at ZORA/PBE/TZP level of theory. (Right top and bottom) QTAIM topology of $[Cf^{VI}O_2\text{-}L]^0$ complex (orange-Cf, red-oxygen, grey-carbon, white-hydrogen, blue-nitrogen)

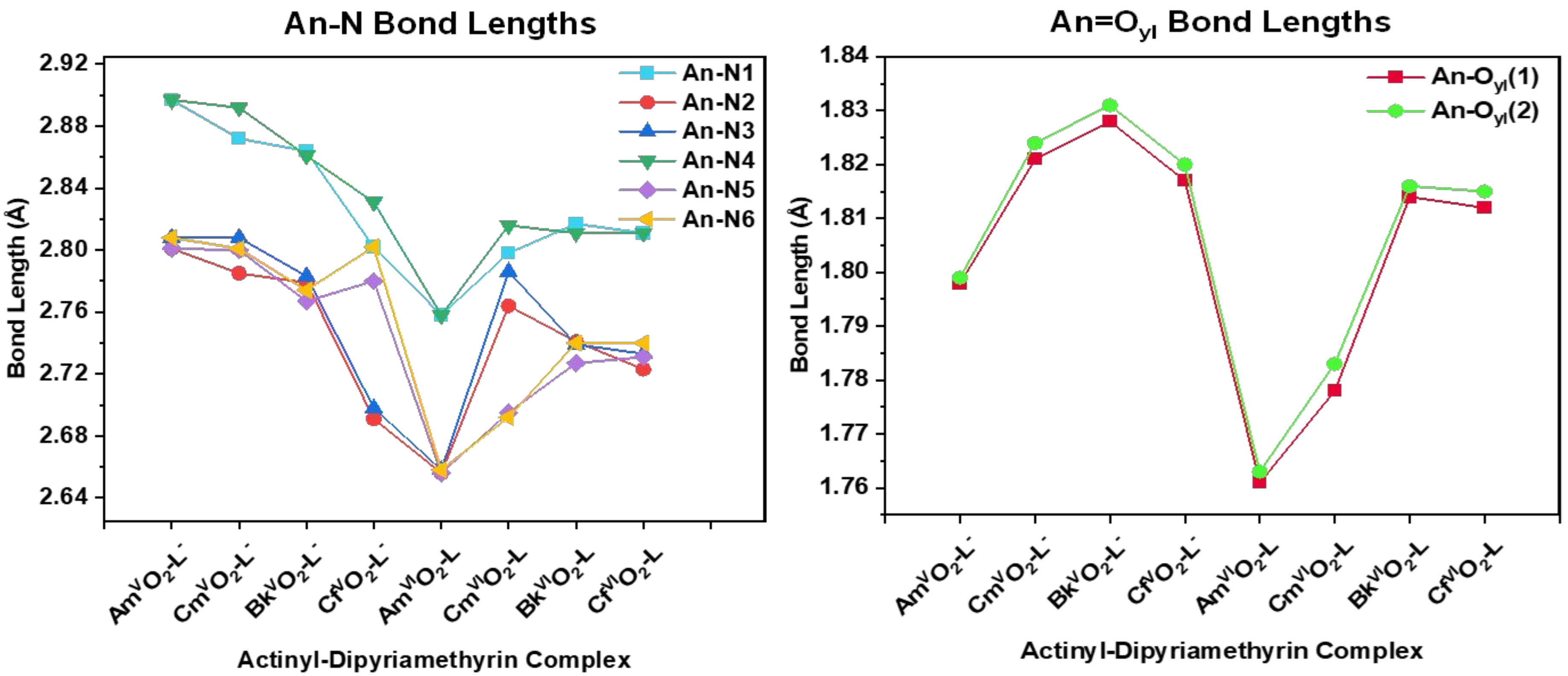

Figure 2. The An-N and An=O_{yl} bond lengths in the actinyl-dipyriamethyrin complex.

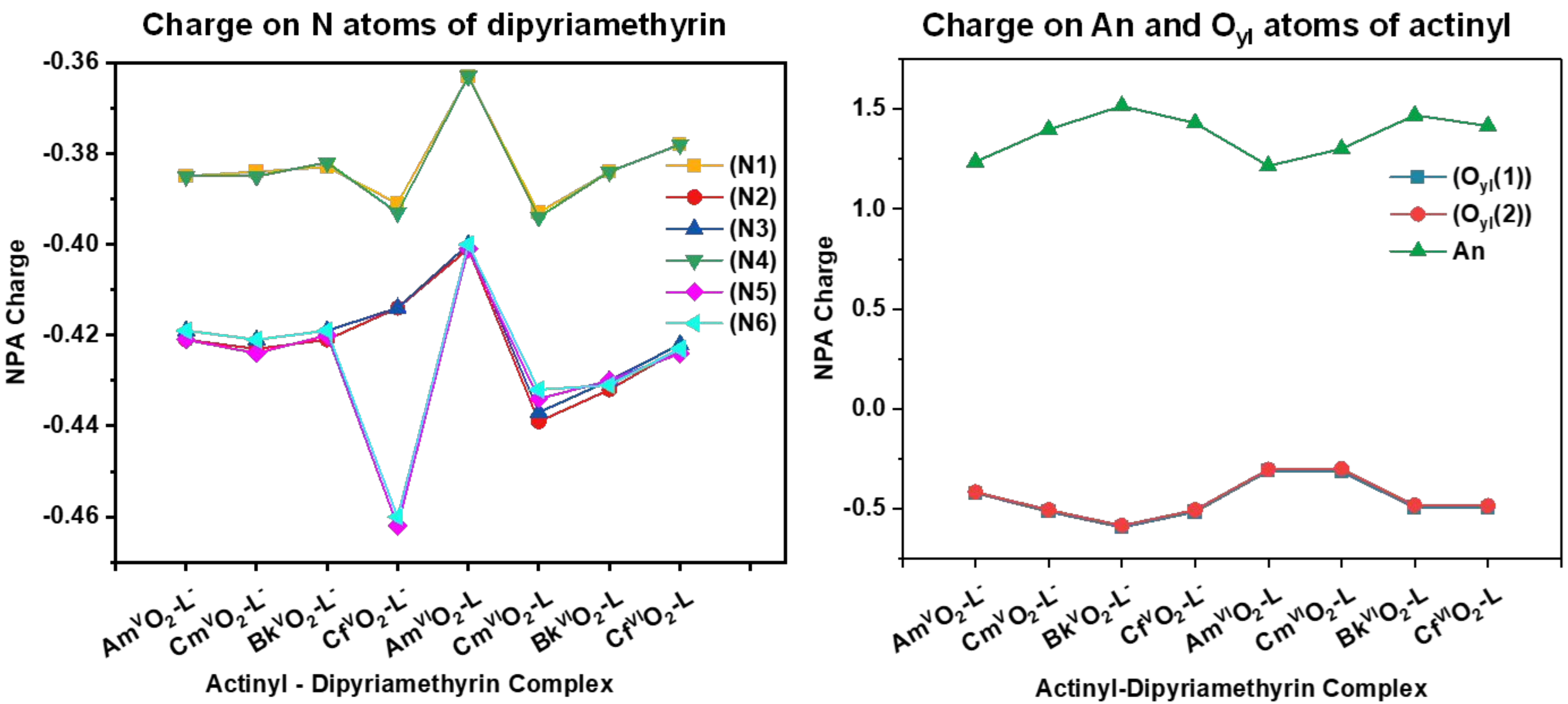

Figure 3. The NPA charge (atomic units) on the nitrogen atoms (left) and on the actinyl atoms (right) in the actinyl-dipyriamethyrin complex.

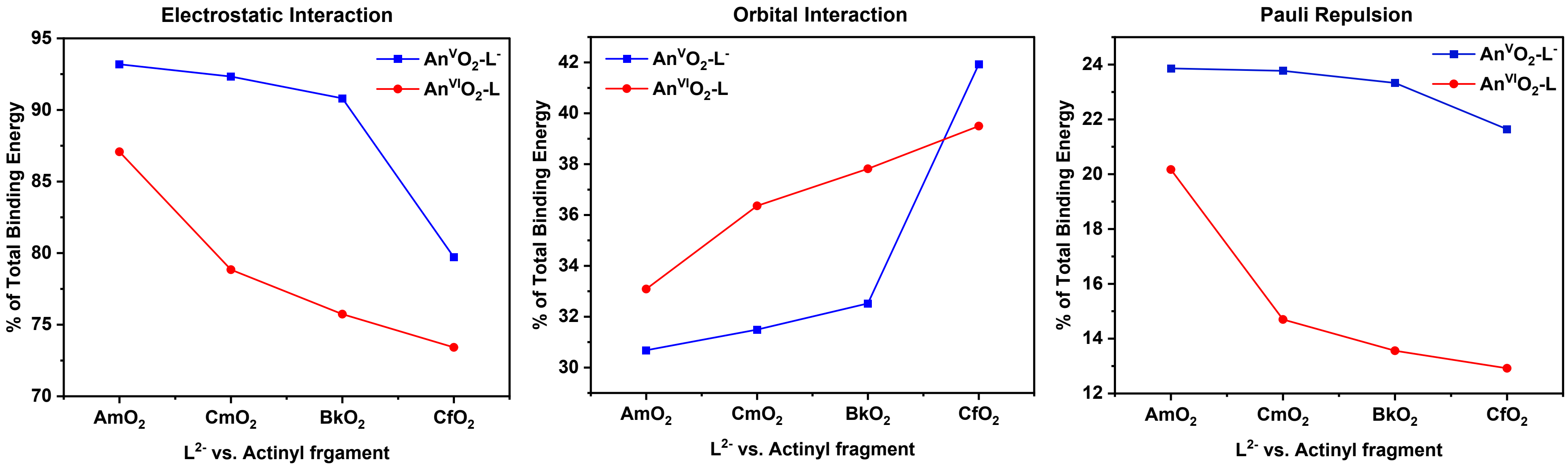

Figure 4. EDA results (kcal/mol) for the actinyl (V and VI) complexes in the gas phase at the PBE/TZP level of theory.

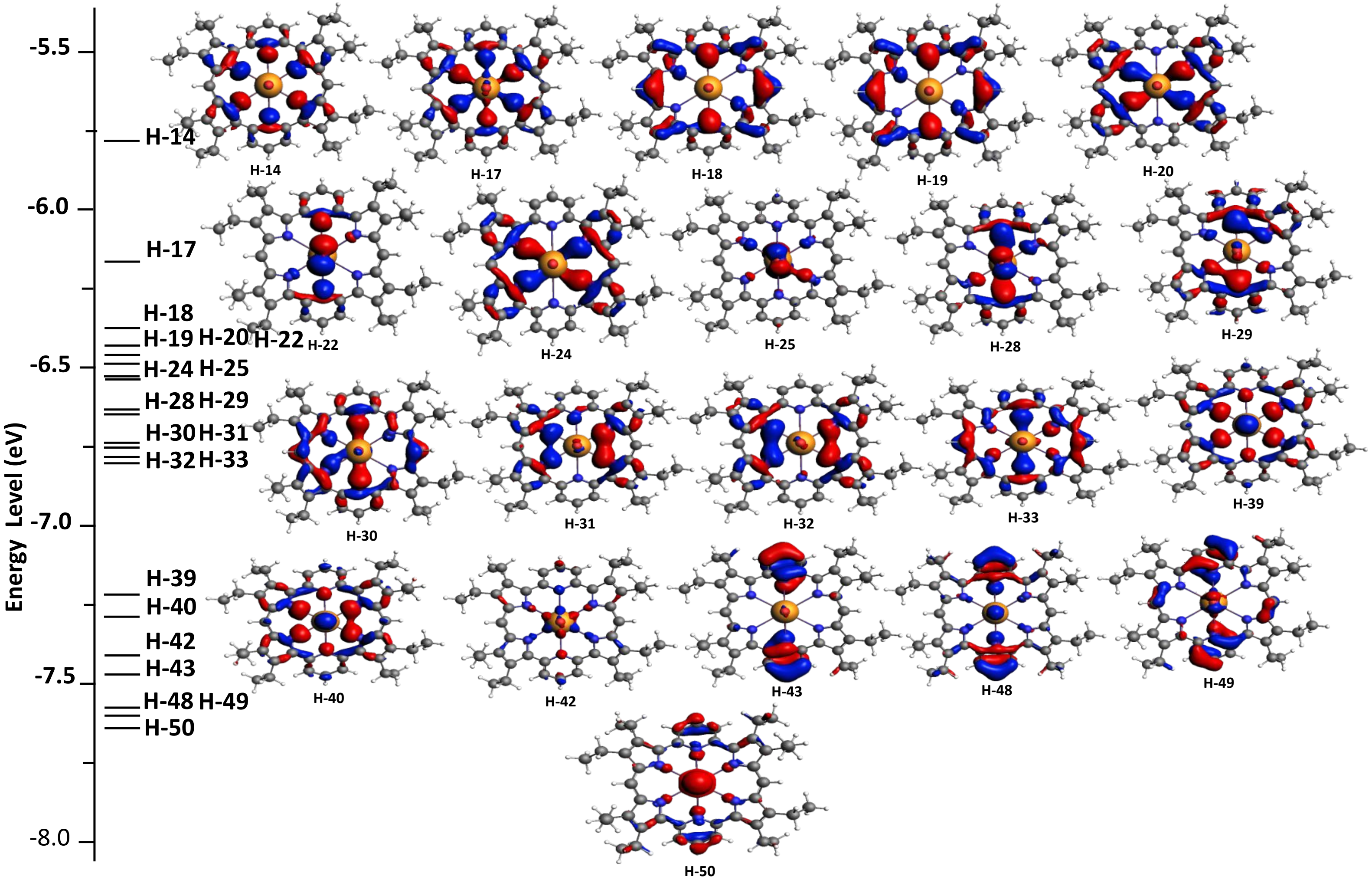

Figure 5. The MOs that represent the stabilizing actinyl-ligand interactions for Cf$^{VI}O_2$-L complex (isovalue is 0.03 a.u.). H represents HOMO.